Journal of Materials Science: Materials in Electronics (2018) 29:6870–6878
https://doi.org/10.1007/s10854-018-8673-4

# Microstructure, enhanced piezoelectric, optical and magnetic properties of Mn substituted $BiFeO_3$ film synthesized by chemical method

Xiaoling Deng[1,2] · Wei Wang[1,2] · Rongli Gao[1,2] · Wei Cai[1,2] · Gang Chen[1,2] · Chunlin Fu[1,2]

Received: 1 November 2017 / Accepted: 24 January 2018 / Published online: 5 February 2018


**Abstract**
Very thin and high transparent manganese (Mn) substituted bismuth ferrite ($BiFe_{1-x}Mn_xO_3$—BFMO) ($x=0$, 0.02, 0.04, 0.06, 0.08, 0.10) films deposited on the $SnO_2$:F (FTO)/glass substrate were synthesized by chemical solution deposition technique. The effect of Mn substitution on the microstructure, piezoelectric, optical and magnetic properties was systematically investigated. X-ray diffraction and Raman spectra analysis revealed that the structure transition and lattice distortion of $BiFeO_3$ (BFO) thin film occurred with Mn substitution. SEM images demonstrated that the average grain size of Mn substituted BFO thin film increased with increase of Mn substitution and EDS results confirmed the element composition with presence of Mn in the synthesized thin film. The piezoresponse of BFMO thin film increased with increase of Mn substitution and when Mn substitution $x=0.10$, the maximum $d_{33,eff}$ reached to 41.81 pm/V, which is almost 125% higher than the pure BFO thin film. The transmittance and optical band gap decreased with increase of Mn substitution. The BFO thin film with Mn substitution $x=0.10$ also showed a lower band gap of 2.64 eV. Furthermore, the Mn substituted BFO thin film show a much higher saturated magnetization compared to pure BFO thin film due to enhanced magnetically driven distortion of spiral spin cycloid induced by Mn substitution.

## 1 Introduction

Multiferroic materials, which can couple at least two of ferroelectricity, (anti)ferromagnetism and ferroelasticity, have drawn lots of attentions due to their promising application in nonvolatile ferroelectric random access memory, transducer and spintronics [1–3]. Among them, bismuth ferrite ($BiFeO_3$, short for BFO) is the rare one exhibiting antiferromagnetic and ferroelectric properties at room temperature and is considered as the one of the most promising candidates for practical application due to its high Curie ferroelectric temperature ($T_C$ ~850 °C) and Néel temperature ($T_N$ ~370 °C) [4, 5], and large remnant polarization ($P_r$) ~100 μC/cm$^2$ [6]. However, the well known problem of BFO thin film is the high leakage current density, caused by the defect (oxygen vacancy) and nonstoichiometry, severely limits its practical application. The problem of nonstoichiometry mainly resulted from volatilization of $Bi^{3+}$ in the annealing process could be avoided by excess addition of raw materials and decrease of annealing temperature and time, while the oxygen vacancy caused by redox coupling of Fe ions is difficult to be controlled [7, 8].

To overcome that obstacle, various attempts such as optimization of preparation method and parameter, site-engineering and scaling effect, have been performed in recent years. Among those measures, B-site substitution with earth rare elements such as Mn, Ni, Ti, Co, etc, to replace Fe ions has been considered as one of the most effective ways to decrease the leakage current and improve the ferroelectric property of BFO thin film [9–13]. Recently, Naganuma et al. reported that Mn substitution could decrease the leakage current and increase the ferroelectric property of BFO thin film [14]. Dhanalakshmi et al. reported that Mn substitution could significantly improve the dielectric and magnetic property of the BFO nanoceramics [15]. However, there has

✉ Xiaoling Deng
dgxmd@163.com

✉ Chunlin Fu
chlfu@126.com

[1] School of Metallurgy and Materials Engineering, Chongqing University of Science and Technology, Huxi Town, Shapingba, Chongqing 401331, China

[2] Chongqing Key Laboratory of Nano/Micro Composite Materials and Devices, Chongqing 401331, China

been limited report focusing on systematical investigation of the crystal structure, microstructure, piezoelectric, optical and magnetic properties of the Mn-substituted BFO thin films deposited on FTO substrate. To obtain high quality Mn substituted BFO films, chemical solution deposition technique is employed due to its several advantages such as easy substitution, simplicity of preparation process and high deposition rate [16–18], compared to pulsed laser deposition [19], magnetron sputtering [20], molecular beam epitaxy [21], electrophoretic deposition [22]. Moreover, the transparent FTO/glass substrate has been widely used to deposit ferroelectric thin films due to its potential application to synthesize the optoelectronic devices [23, 24].

In our work, the Mn substituted BFO thin film was deposited on the FTO substrate by a chemical solution technique. The effect of transition metal ion (Mn) substitution on the crystal structure, microstructure, piezoelectric, optical and magnetic properties of BFO thin films was systematically investigated.

## 2 Experimental

$BiFe_{1-x}Mn_xO_3$ (BFMO) ($x = 0$, 0.02, 0.04, 0.06, 0.08, 0.10) thin films were deposited onto FTO/glass substrates by chemical solution deposition method. Bismuth nitrate [$Bi(NO_3)_3{\cdot}5H_2O$], ferric nitrate [$Fe(NO_3)_3{\cdot}9H_2O$] and manganese acetate [$(C_2H_3O_2)_2Mn{\cdot}4H_2O$] were dissolved into 2-methoxyethanol/acetic acid with the atomic ratio of 1.05:1–*x*:*x* ($x = 0$, 0.02, 0.04, 0.06, 0.08, 0.10). 5 mol% of excess Bi was added to compensate for bismuth loss during the annealing process. The volume ratio of 2-methoxyethanol/acetic acid is 3:2. Then the solution was stirred for 3 h at 85 °C to obtain a homogeneous precursor. The concentration of the final solution is 0.3 mol/L. Then the thin film was deposited on FTO/glass substrate by spin coating at 3000 rpm for 60 s followed by a pyrolysis process on a hot plate at 250 °C for 10 min to decompose the remaining organic compounds. The spin coating and pyrolysis process was repeated five times to get a desired film thickness. Finally, the thin films were annealed via a rapid thermal annealing furnace at 600 °C for 10 min with a heating rate of 100 °C/min in air.

The crystal structure of crystallized thin films was characterized by X-ray diffraction (XRD, D8 Advance, Bruker, Germany) with Cu Kα radiation ($\lambda = 0.154056$ nm). Detailed phase of thin films was analyzed by Raman spectroscopy under an excitation wavelength of 532 nm using a YAG as a source. The surface morphology and thickness of the thin films were performed using field-emission scanning electron microscope (FE-SEM, S-4800, Hitachi, Japan). The chemical composition was confirmed by energy-dispersive X-ray spectroscopy (EDS, Oxford, UK). The ferroelectric hysteresis loop and piezoelectric characteristics were measured by piezoelectric force microscope (Nanoscope V Multimode, Bruker, Germany). The driving amplitude was 5 V. The local piezoelectric hysteresis loop was measured by applying a dc bias ranging from − 10 to + 10 V. The optical transmission over the ultraviolet–visible (UV–vis) range was measured by UV–vis spectrophotometry (TU1810, Persee, China). The magnetic properties were studied by using vibrating sample magnetometer (VSM, VSM-300, YP Magnetic Technology Development CO. LTD, China).

## 3 Results and discussion

### 3.1 Microstructure

Figure 1 shows the XRD patterns of Mn substituted BFO thin films annealed at 600 °C in air. It is clear that all samples show well-developed crystalline peaks of the rhombohedral BFO phase (JCPD: 071-2494) indexed to

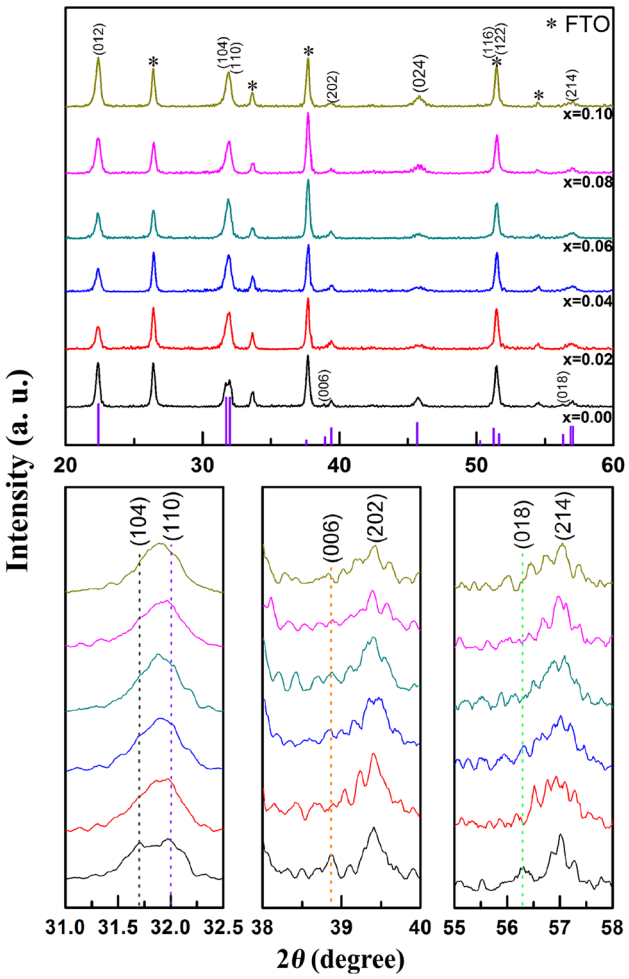


**Fig. 1** XRD patterns of Mn substituted BFO thin films annealed at 600 °C for 10 min

*R3*c-161 group. No secondary phase is observed indicating that the $Mn^{2+}$ has been successfully substituted to replace the $Fe^{3+}$. Without Mn substitution, it is obvious that (104) and (110) peaks are clearly separated and minor peaks of (006) and (018) are existed, as shown in the corresponding magnified view of XRD patterns. With increase of Mn substitution, the diffraction intensity of (104) decreases; peaks of (104) and (110) are merged to a single peak and the main peak shits to the higher angle; (006) and (018) peaks almost disappear. All of these observations might suggest that the Mn substitution induces a lattice distortion and structure transition which may be from rhombohedral towards to the orthorhombic or tetragonal structure [25, 26]. Moreover, the merged peak shifts towards to lower angle with increase of Mn substitution due to the different ion radius of $Mn^{2+}$ (0.645 Å) and $Fe^{3+}$ (0.782 Å) [27].

In order to further analyze the influence of Mn substitution on the crystal structure of BFO thin film, the lattice parameters and average grain size of Mn substituted BFO thin films are calculated and shown in Fig. 2. The c/a ratio decreases with increase of Mn substitution while the cell volume increases, as can be observed in Fig. 2a, implying that the various growth rate of plane which further affects the grain shape. It is also obvious that the (012) orientation is varied with increase of Mn substitution. The (012)-orientation of the BFMO thin films were calculated by the equation as following [28]:

$$\alpha_{(102)} = \frac{I_{(102)}}{I_{(102)} + I_{(104)} + I_{(110)}} \quad (1)$$

where $\alpha_{(012)}$ is the orientation degree of peak (012), $I_{(012)}$, $I_{(104)}$ and $I_{(110)}$ are the intensity of the peak (012), (104) and (110), respectively. The calculated $\alpha_{(012)}$ according to the Eq. (1) is shown in Fig. 2b. Obviously, the Mn substitution induces a different grain orientation growth in BFO thin film, which is similar with the result reported by Li et al. [10]. The average grain size of Mn substituted BFO thin films were calculated according to the full width at half maximum data in XRD patterns by the Scherrer equation [29]:

$$D = \frac{K\lambda}{\beta cos\theta} \quad (2)$$

where $D$ is the crystallite size (nm), $K$ is the shape factor (0.89), $\lambda$ is the wavelength of the X-rays ($\lambda = 0.15406$ nm for Cu Kα radiation), $\beta$ is the width of the diffraction peak at half maximum for the diffraction angle $2\theta$. According to Eq. (2), the average grain size of Mn substituted BFO thin films is found to be increased from 20 to 45 nm, as shown in Fig. 2b, indicating that the Mn substitution could promote the grain growth. Similar results have been reported by Liu et al. [30] and Huang et al. [31].

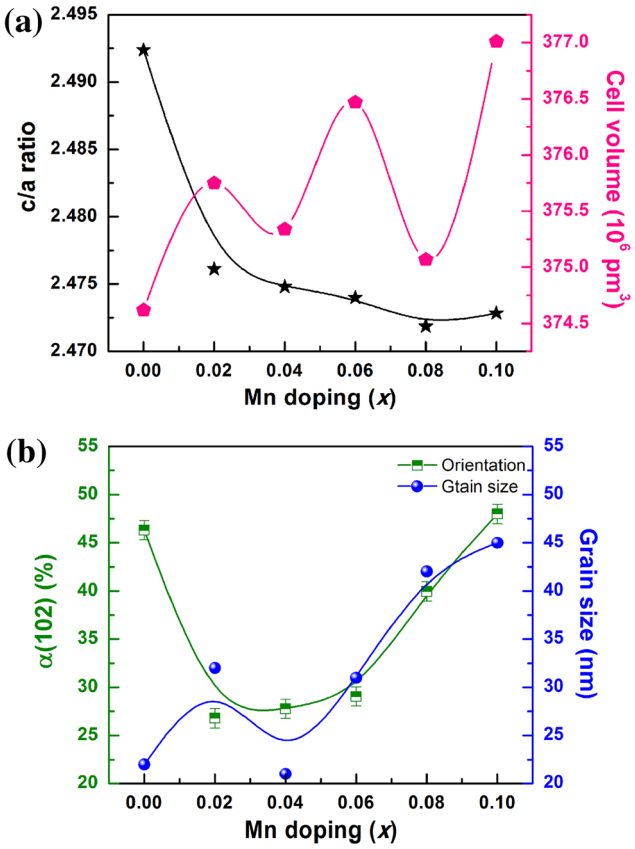


**Fig. 2** **a** Calculated lattice parameters of *c/a* ratio and unit cell volume; **b** orientation degree of peak (102) and average grain size of Mn substituted BFO thin films

In order to derive more detailed crystal structure information of epitaxial Mn substituted BFO thin films, the Raman spectra of as prepared thin films was performed, as shown in Fig. 3. Each peak observed in the Raman spectrum was applied the Gauss-fitting. According to the group theory, the rhombohedral structure BFO thin film with *R3*c space group has 13 ($\Gamma = 4A_1 + 9E$) Raman active modes [32, 33]. As can be observed in Fig. 3, without Mn substitution, the BFO thin film clearly shows four $A_1$ modes at 141, 172, 219 and 437 $cm^{-1}$, and four E modes at 265, 341, 524 and 607 $cm^{-1}$, indicating that the obtained pure BFO thin film grows with rhombohedral structure [34]. With increase of Mn substitution, (i) $A_1$-1 and $A_1$-2 modes corresponding to the Bi–O vibration are gradually suppressed and promoted, respectively, which may be due to the change of dispersion or number of Bi–O bond length resulted from the Mn substitution, indicating that the structure transition occurs [35]; (ii) $A_1$-1 mode gradually shift towards to lower wave number (141.5–138.3 $cm^{-1}$); (iii) the intensity of $A_1$-4 and E-9 modes corresponding to Fe–O bonds significantly increase due to the Jahn–Teller distortion, which may be resulted from the symmetric and asymmetric stretching vibrations of

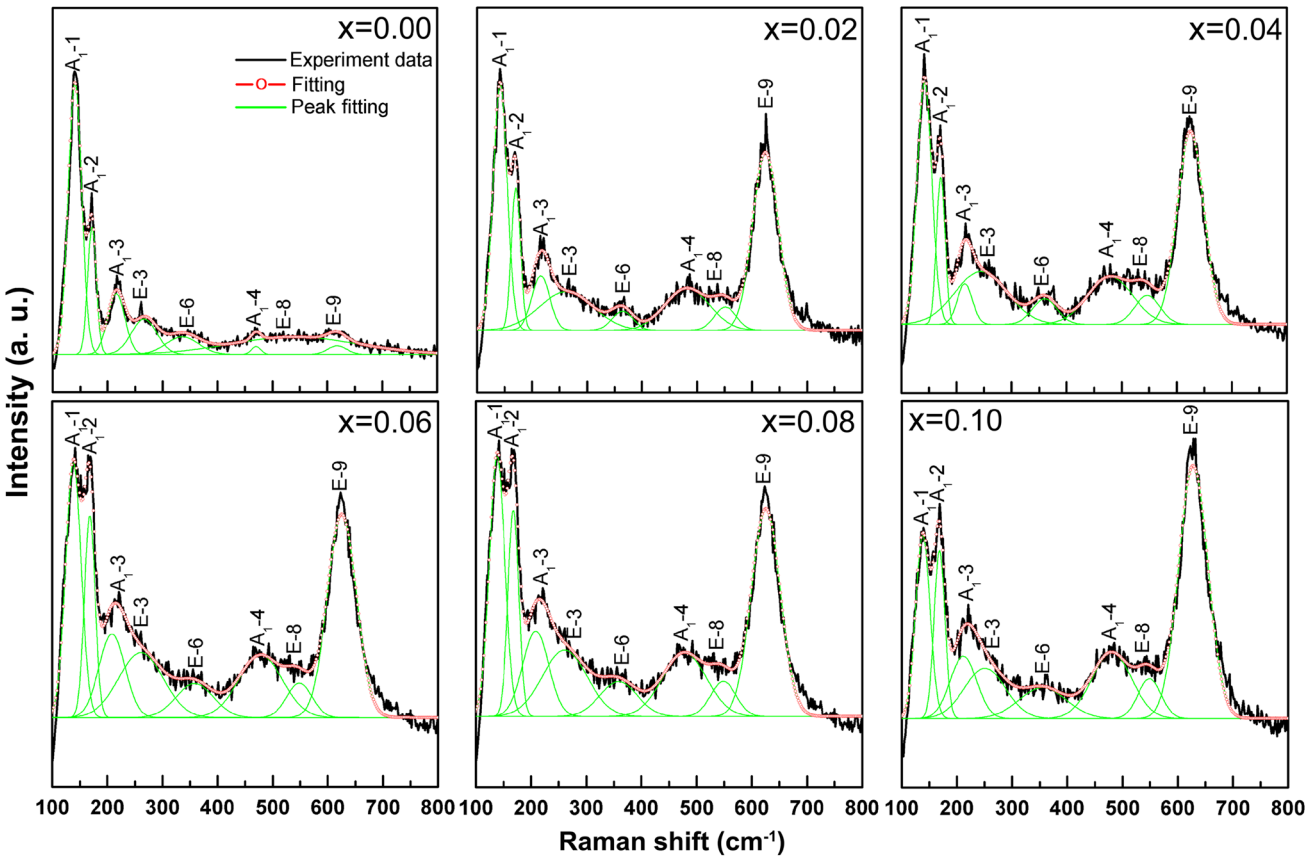


**Fig. 3** Raman spectrum of Mn substituted BFO thin films

Fe–O bonds in (Fe,Mn)$O_6$ octahedra [36, 37]. All of these observations become more and more evident with increase of Mn substitution. Hence, it can be confirmed that a structure transition from rhombohedral to coexistence of rhombohedral and tetragonal occurs due to the Mn substitution [38]. It is well known that morphotropic phase boundary (MPB) plays an important role in enhancement of piezoelectric property of ferroelectric materials. The as-synthesized Mn substituted BFO thin film with structure transition which is similar to MPB effect existed in Pb(Zr,Ti)$O_3$ (PZT) based ceramics is expected to show a much better piezoelectric property.

Figure 4 shows the surface morphology and cross-sectional SEM images of Mn substituted BFO thin films. The thickness of BFO thin film is almost 150 nm as observed from the inset figure of Fig. 4a. It is obvious that all obtained BFMO thin films show dense and crack-free structure with well-shaped grains. With increase of Mn substitution, the average grain size firstly decreases and subsequently increases, indicating that small amount ($x \leq 0.04$) of Mn substitution could restrain the grain growth rate while large amount Mn substitution could promote the grain growth. Moreover, it is observed that when the Mn content $x \geq 0.06$, the grain seems to merge together to form a large grain with recognized grain boundary and when $x = 0.10$, some voles appear. The average grain size of each Mn substituted BFO thin film was estimated to be 66.56, 58.19, 54.31, 100.52, 186.27 and 200.74 nm through the linear intercept method. Since the grains merge together, it is acceptable that a tolerance of $\pm 5$ nm is existed in average grain size when $x \geq 0.06$. Obviously, the change trend of average grain size is consistent with the result calculated by the Scherrer equation (as shown in Fig. 2b) but much larger than that. This is due to the stress existed in BFO thin film which can not be considered in Scherrer equation. It is well known that the grain boundary density and surface morphology greatly affect the electrical and optical properties of BFO thin film.

The chemical composition of 10% Mn substituted BFO thin film was confirmed by EDS technique, and the result is shown in Fig. 5. The results clearly confirm the presence of essential (Bi, Fe, O) and substituted (Mn) elements. The inset element mapping shows that the Bi (green), Fe (red), Mn (blue) and O (purple) elements are uniformly distributed in the synthesized sample. These results clearly indicate that Mn has been uniformly substituted in BFO thin film, which is in good agreement with XRD results.

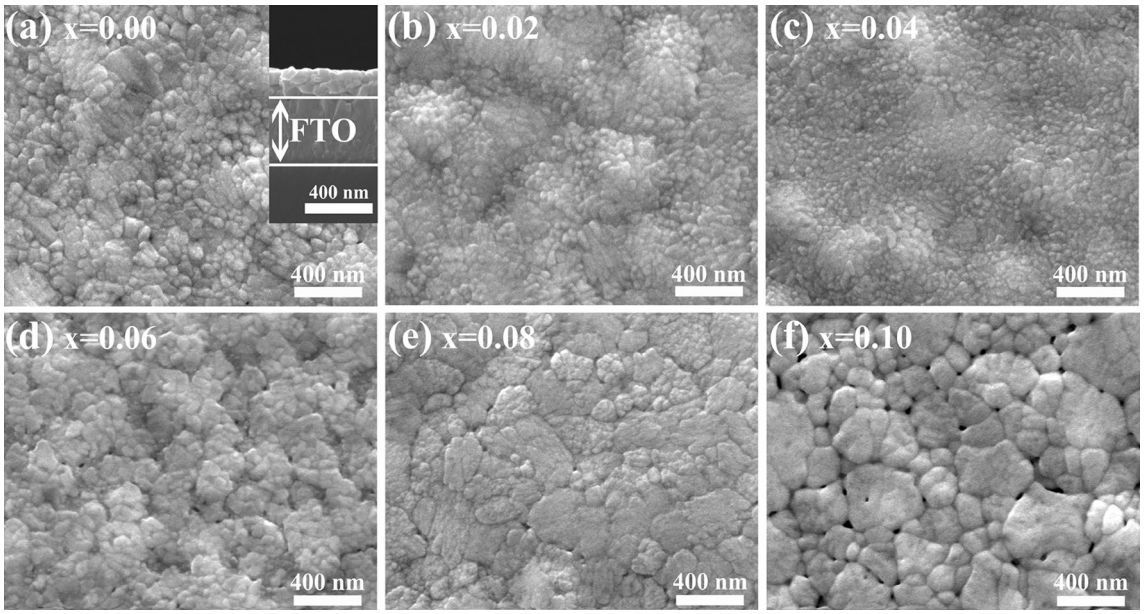


**Fig. 4** Top and cross-sectional SEM images of Mn substituted BFO thin films

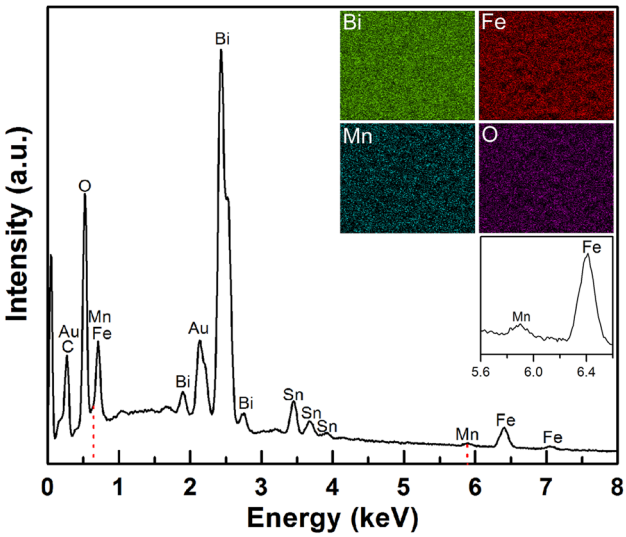


**Fig. 5** EDS spectroscopy pattern of 10% Mn substituted BFO thin film. Inset figures are the element mapping of Bi, Fe, Mn and O and magnified view in the vicinity of energy around 6 keV. (Color figure online)

## 3.2 Properties of thin film

### 3.2.1 Piezoelectric properties

Figure 6 demonstrates the local piezoresponse and phase curves of Mn substituted BFO thin films under a dc bias ranged from − 10 to 10 V. According to Fig. 6a, it is noted that all samples exhibit well-shaped butterfly loops corresponding to the representative strain–electric field (S–E) curve of piezoelectric materials. It is obvious that the obtained amplitude of Mn substituted BFO thin film increases with increase of Mn substitution, indicating that a higher piezoresponse. The corresponding piezoelectric coefficient ($d_{33,\text{eff}}$) was calculated by the known equation as shown following [39]:

$$d_{33,eff} = \frac{\sigma \times A}{V_{ac}} \tag{3}$$

where σ is the deflection sensitivity, $A$ is the amplitude and $V_{ac}$ is the driving ac voltage. The calculated $d_{33,\text{eff}}$ of each Mn substituted BFO thin film is shown in Table 1. It is clear that the $d_{33,\text{eff}}$ of Mn substituted BFO thin film significantly increases with increase of Mn substitution. When Mn substitution $x = 0.10$, the $d_{33,\text{eff}}$ of BFMO thin film reaches the maximum value of 41.81 pm/V, which is almost 125% higher than the pure BFO thin film. This may be attributed to two reasons: (i) the structure transition induced by Mn substitution; (ii) the significantly increased grain size. It is well known that MPB plays an important role in the significantly enhanced piezoelectric property of representative piezoelectric materials such as PZT. The Mn substitution results in a structure transition so that a significant enhancement of piezoelectric coefficient is obtained. Secondly, the increased grain size leads to a decrease of grain boundary density so that the domain wall mobility increases due to less restriction by grain boundaries [40, 41].

Figure 6b shows the corresponding piezoresponse phase curves of Mn substituted BFO thin films. It is clear that the coercive field increases with increase of Mn substitution.

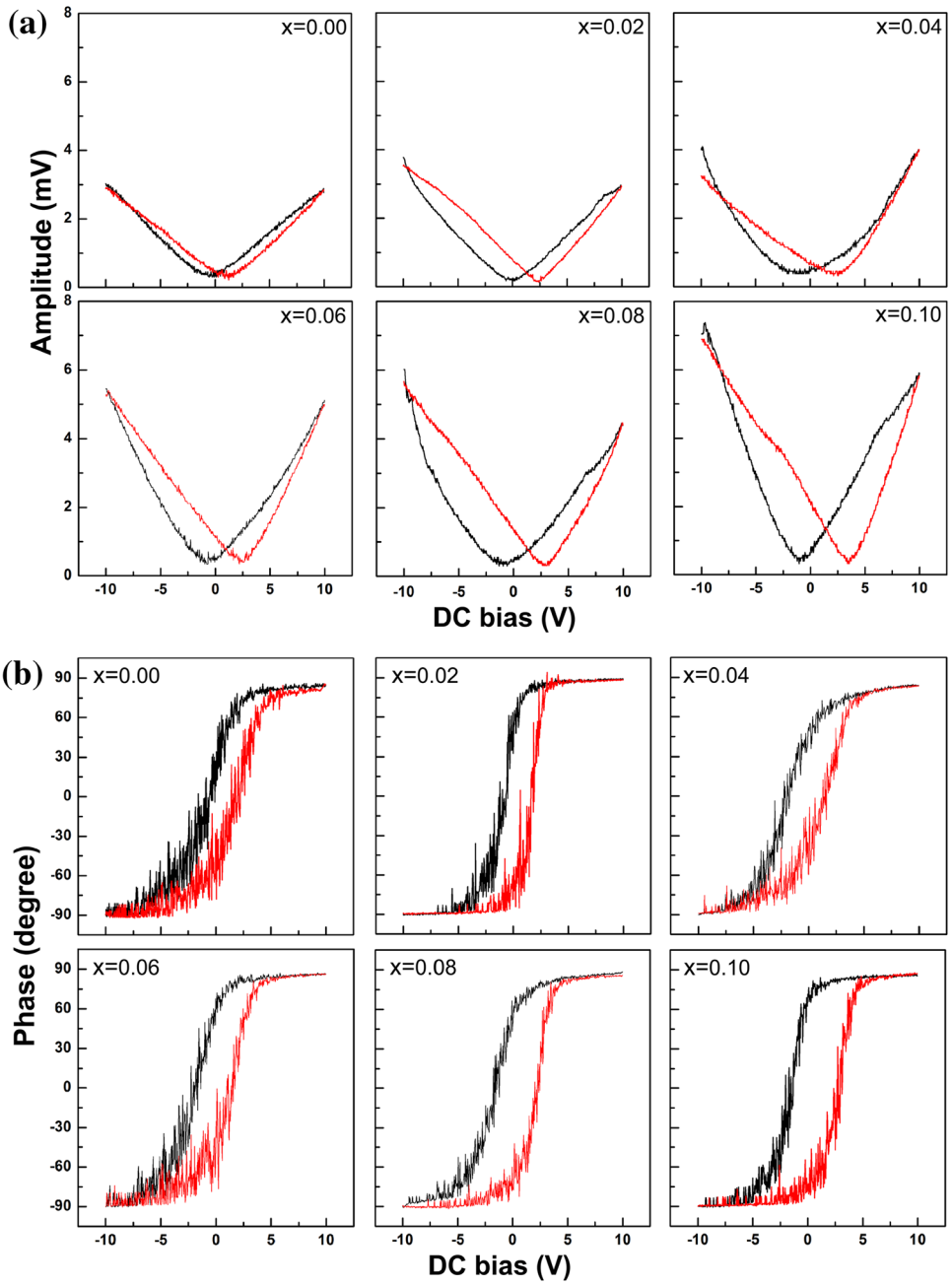


**Fig. 6** Piezoresponse **a** amplitude and **b** phase curves of Mn substituted BFO thin films

**Table 1** Normalized coercive field, piezoelectric coefficient and difference in PR phase of Mn substituted BFO thin films

| Mn substitution ($x$) | 0 | 0.02 | 0.04 | 0.06 | 0.08 | 0.10 |
|---|---|---|---|---|---|---|
| Normalized $V_c$ | 1.00 | 1.04 | 1.49 | 1.55 | 1.75 | 1.83 |
| $d_{33,\text{eff}}$ (pm/V) | 18.53 | 23.02 | 24.45 | 33.34 | 36.73 | 41.81 |
| $\Delta\Phi$ (°) | 174.75 | 179.51 | 174.05 | 176.89 | 178.51 | 175.43 |

The average coercive filed $[V_c = 1/2(V_c^+ - V_c^-)]$ was estimated from the curves and the normalized result is shown in Table 1. It is found that the coercive field of Mn substituted BFO thin film increases with increase of Mn substitution, indicating that a higher electric field is needed to switch the domain which is mainly due to the significantly increased grain size. Moreover, the hard doping effect due to Mn substitution and existence of defects such as oxygen vacancy is helpful to pin the domain wall so that prevent the domain switching leading to an increase of coercive

filed, which is similar to the reported Mn substituted piezoelectric materials [31, 42, 43]. The difference of piezoelectric phase [$\Delta\Phi = 1/2(\Phi^{+} - \Phi^{-})$] was estimated as shown in Table 1. It is clear that all samples show similar value in range of 174°–180°, indicating that a 180° domain switching occurs under the same dc bias.

### 3.2.2 Optical properties

Figure 7 shows the UV–vis transmittance spectra and $(\alpha hv)^2$ versus $hv$ curves of Mn substituted BFO thin films annealed at 600 °C in air. As can be seen from Fig. 7a, all samples show interference fringes and high transparency ranged from 60–90% in visible and near infrared region. Moreover, an obvious transition occurred in 450–550 nm range, which corresponds to electronic transitions involving charge transfer from valence-band O 2p states to conduction-band Fe 3d states, shifts to the higher wavelength due to the increase of grain size resulted from Mn substitution [44]. It is obvious that Mn substitution can decrease the transmittance of BFO thin film. Normally, the increase of grain size leads to a decrease of grain boundary density so that less scattering occurs [10]. Therefore, the decrease of transmittance in this work indicates the higher absorption of visible light and ultraviolet light of BFO thin film resulted from effect of Mn substitution. The optical band gap $E_g$ of each thin films was estimated by classical Tauc relation as shown following:

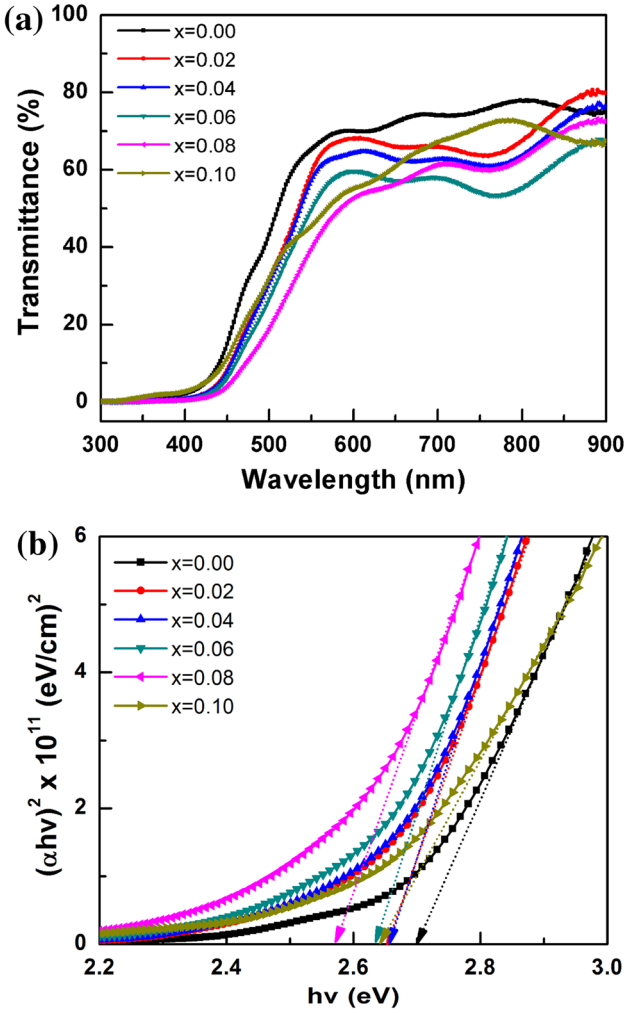


**Fig. 7** **a** Optical transmittance and **b** $(\alpha hv)^2$ versus $hv$ curves of Mn substituted BFO thin films

$$\alpha hv = \mathrm{A}\left(hv - E_g\right)^n \tag{3}$$

where A is a constant, $hv$ is the photon energy, $E_g$ is the band gap and $\alpha$ is the absorption coefficient calculated from the expression $a = (1/\mathrm{d})\ln[(1-\mathrm{R})^2/\mathrm{T}]$, $n$ is 2 as for a direct band gap. Figure 7b shows the curve extrapolated from the linear portion of $(\alpha hv)^2$ versus photon energy ($hv$). As can be seen from Fig. 7b, it is clear that Mn substitution is helpful to narrow the band gap of BFO thin film. The estimated band gap of each Mn substituted BFO thin film is shown in Table 2. Obviously, with increase of Mn substitution, the band gap firstly decreases to 2.57 eV when $x = 0.08$ and then increases to 2.64 eV when $x = 0.10$. The decrease of band gap is mainly due to the significant increase of grain size and intrinsic density of free electrons [10, 26]. Moreover, the decrease of band gap can be attributed to the rearrangement of molecular orbitals and distortion induced by the Fe–O octahedral [45, 46].

### 3.2.3 Magnetic properties

Figure 8 shows room temperature magnetic hysteresis loops of Mn substituted BFO thin films measured under a maximum magnetic field of 5 kOe. All films exhibit weak ferromagnetic behaviors with a saturation magnetization in high magnetic filed. It is noted that saturated magnetization of BFO thin films is significantly influenced by Mn substitution and increases with increase of Mn content. When Mn substitution $x$ is increased to 0.10, the saturated magnetization of Mn substituted BFO thin film is increased to 0.3258 emu/g, which is almost three times higher than the pure BFO thin film (0.0913 emu/g). The magnetization enhancement of Mn

**Table 2** Optical band gap ($E_g$) of Mn substituted BFO thin films

| Mn substitution ($x$) | 0 | 0.02 | 0.04 | 0.06 | 0.08 | 0.10 |
|---|---|---|---|---|---|---|
| $E_g$ (eV) | 2.70 | 2.65 | 2.66 | 2.63 | 2.57 | 2.64 |

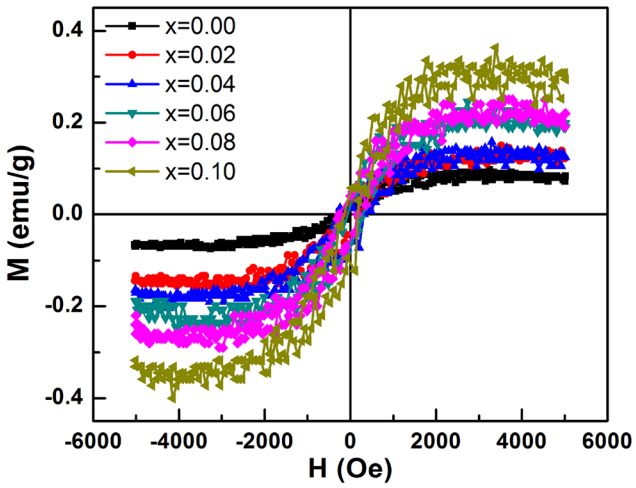


**Fig. 8** Magnetic hysteresis loops of Mn substituted BFO thin films

substituted BFO thin film is mainly attributed to two aspects. Firstly, it has been reported that structure transition can induce the partial spin rearrangement by influencing the cationic interaction [47]. And according to the Raman result, E-9 mode shifting to higher frequency indicates that the change of Fe–O bond which leads to change of G-type antiferromagnetic ordering and the $Fe^{3+}$–O–$Fe^{2+}$ bond angle. Hence, the magnetic property of Mn substituted BFO thin film is enhanced and the higher structure transition due to higher Mn substitution leads to a higher magnetization. Secondly, Mn substitution can induce the spin cycloid ordering distortion by suppressing $Fe^{2+}$ influence on canting of $Fe^{3+}$ spin resulting in magnetization enhancement [48]. Moreover, it has been widely reported that the magnetic property of BFO thin film can be influenced by the grain size, especially when the grain size is less than antiferromagnetic spiral wavelength of 62 nm [49]. It means that with decrease of grain size, the BFO thin film should show higher magnetization value. However, in present study, the effect of grain size on the magnetic property of Mn substituted BFO thin films seem not obey that rule because the abnormal grain growth observed from SEM image may lead to a different magnetic property. Similar result has also been reported by elsewhere [50].

## 4 Conclusions

In summary, $BiFe_{1-x}Mn_xO_3$ ($x = 0.00$, 0.02, 0.04, 0.06, 0.08, 0.10) thin films deposited on FTO/glass substrate were successfully obtained by using a chemical solution method. Structure analyses reveal that Mn substitution can induce a structure transition by the coexistence of rhombohedral and tetragonal phases and promote the grain growth. With the crystal structure transition and increased grain size, the piezoelectric, optical and magnetic properties of BFO thin film are effectively enhanced. Among these films studied, the 10% Mn substituted BFO thin film exhibits better piezoelectric coefficient, better saturated magnetization and lower band gap. All above results demonstrate the promising application of 10% Mn substituted BFO thin film in piezoelectric, optoelectronic and spintronic devices.

**Acknowledgements** This work was supported by the National Natural Science Foundation of China (Grant Nos. 51372283, 51402031, 61404018), Chongqing Research Program of Basic Research and Frontier Technology (Grant Nos. CSTC2016jcyjA0175, CSTC2015jcyjA50015, CSTC2016jcyjA0349), the Program for Innovation Teams in University of Chongqing, China (Grant No. CXTDX201601032), the Science and Technology Innovation Project of Social Undertakings and People's Livelihood Guarantee of Chongqing, China (Grant No. cstc2017shmsA0192) and the cooperative project of academician workstation of Chongqing University of Science Technology (Grant No. CKYS201504).

## References

1. S.Y. Yang, F. Zavaliche, L. Mohaddes-Ardabili, V. Vaithyanathan, D.G. Schlom, Y.J. Lee, Y.H. Chu, M.P. Cruz, Q. Zhan, T. Zhao, R. Ramesh, Appl. Phys. Lett. **87**, 102903 (2005)
2. M.M. Kumar, V.R. Palkar, K. Srinivas, S.V. Suryanarayana, Appl. Phys. Lett. **76**, 126468 (2000)
3. Y.H. Chu, L.W. Martin, M.B. Holcomb, R. Ramesh, Mater. Today **10**, 16 (2007)
4. R. Ramesh, N. Spaldin, Nat. Mater. **6**, 21 (2007)
5. C. Catalan, J.F. Scott, Adv. Mater. **21**, 2463 (2009)
6. J. Wang, J.B. Neaton, H. Zheng, V. Nagarajan, S.B. Ogale, B. Liu, D. Viehland, V. Vaithyanathan, D.G. Schlom, U.V. Waghmare, N.A. Spaldin, K.M. Rabe, M. Wutting, R. Ramesh, Science **299**, 1719 (2003)
7. K.Y. Yun, M. Noda, M. Okuyama, Appl. Phys. Lett. **83**, 3981 (2003)
8. J.G. Wu, J. Wang, D.Q. Xiao, J.G. Zhu, J. Appl. Phys. **110**, 064104 (2011)
9. B. Xu, D. Wang, J. Guez, L. Bellaiche, Adv. Funct. Mater. **25**, 552 (2015)
10. J. Li, K. Liu, J. Xu, L. Wang, L. Bian, F. Xu, J. Mater. Sci. Res. **2**, 75 (2013)
11. D.K. Mishra, X. Qi, J. Alloys Compd. **504**, 27 (2010)
12. W. Cai, C. Fu, R. Gao, W. Jiang, X. Deng, G. Chen, J. Alloys Compd. **617**, 240 (2014)
13. G. Dong, G. Tan, Y. Luo, W. Wang, H. Ren, A. Xia, J. Alloys Compd. **654**, 419 (2016)
14. H. Naganuma, J. Miura, S. Okamura, Appl. Phys. Lett. **93**, 052901 (2008)
15. B. Dhanalakshmi, K. Pratap, B. Parvatheeswara Rao, P.S.V. Subba, Rao, J. Alloys Compd. **676**, 193 (2016)
16. M. Salavati-Niasari, F. Soofivand, A. Sobhani-Nasab, M. Shakouri-Arani, M. Hamadanian, S. Bagheri, J. Mater. Sci. Mater. Electron. **28**, 14965 (2017)
17. A. Sobhani-Nasab, A. Ziarati, M. Rahimi-Nasrabadi, M.R. Ganjali, A. Badiei, Res. Chem. Intermed. **43**, 6155 (2017)
18. A. Ziarati, A. Sobhani-Nasab, M. Rahimi-Nasrabadi, M.R. Ganjali, A. Badiei, J. Rare Earth **35**, 374 (2017)
19. J. Zhu, W.B. Luo, Y.R. Li, Appl. Surf. Sci. **255**, 3466 (2008)

20. X. Deng, J. Huang, Y. Sun, K. Liu, R. Gao, W. Cai, C. Fu, J. Alloys Compd. **684**, 510 (2016)
21. L.W. Martin, D.G. Schlom, Curr. Opin. Solid State Mater. Sci. **16**, 199 (2012)
22. K. Liu, W. Cai, C. Fu, K. Lei, L. Xiang, X. Gong, J. Alloys Compd. **605**, 21 (2014)
23. Z.D. Wang, Z.Q. Lai, Z.G. Hu, J. Alloys Compd. **583**, 452 (2014)
24. L. Zhang, J. Chen, J. Cao, D. He, X. Xing, J. Mater. Chem. C **3**, 4706 (2015)
25. V.R. Palkar, D.C. Kundaliya, S.K. Malik, J. Appl. Phys. **93**, 4337 (2003)
26. H.B. Sharma, N.B. Singh, K.N. Devi, J.H. Lee, S.B. Singh, J. Alloys Compd. **583**, 106 (2014)
27. S. Gupta, A. Sharma, M. Tomar, V. Gupta, M. Pal, R. Guo, A. Bhalla, J. Appl. Phys. **111**, 064110 (2012)
28. X. Tang, J. Dai, X. Zhu, Y. Sun, J. Alloys Compd. **552**, 186 (2013)
29. M.Y. Shami, M.S. Awanm, M. Anis-ur-Rehman, J. Alloys Compd. **509**, 10139 (2011)
30. W. Liu, G. Tan, G. Dong, X. Yan, W. Ye, H. Ren, A. Xia, J. Mater. Sci. Mater. Electron. **25**, 723 (2014)
31. J. Huang, Y. Wang, Y. Lin, M. Li, C.W. Nan, Appl. Phys. Lett. **106**, 063911 (2009)
32. M.K. Singh, H.M. Jang, S. Ryu, M.H. Jo, Appl. Phys. Lett. **88**, 042907 (2006)
33. S.K. Srivastav, N.S. Gajbhiye, A. Banerjee, J. Appl. Phys. **113**, 203917 (2013)
34. S. Mukherjee, R. Gupta, A. Garg, V. Bansal, S. Bhargava, J. Appl. Phys. **107**, 123535 (2010)
35. F.D. Hardcastle, I.E. Wachs, J. Solid State Chem. **97**, 319 (1992)
36. G. Dong, G. Tan, Y. Luo, W. Liu, A. Xia, H. Ren, Appl. Surf. Sci. **305**, 55 (2014)
37. B. Ramachandran, M.S. Ramachandra Rao, J. Appl. Phys. **112**, 073516 (2012)
38. S. Gupta, M. Tomar, V. Gupta, J. Mater. Sci. **48**, 5997 (2014)
39. R. García, R. Pérez, Surf. Sci. Rep. **47**, 197 (2002)
40. W. Cao, C.A. Randall, J. Phys. Chem. Solids. **57**, 1499 (1996)
41. H.T. Martirena, J.C. Burfoot, J. Phys. C **7**, 3182 (1974)
42. W. Zhu, I. Fujii, W. Ren, S. Trolier-Mckinstry, J. Appl. Phys. **109**, 064105 (2011)
43. L. Luo, D. Zhou, Y. Tang, Y. Jia, H. Xu, H. Luo, Appl. Phys. Lett. **90**, 102907 (2007)
44. P.S.V. Mocherla, C. Karthik, R. Ubic, M.S. Ramachandra Rao, C. Sudakar, Appl. Phys. Lett. **103**, 022910 (2013)
45. P. Tang, D. Kuang, S. Yang, Y. Zhang, J. Alloys Compd. **622**, 194 (2015)
46. P.C. Sati, M. Arora, S. Chauhan, M. Kumarn, S. Chhoker, J. Phys. Chem. Solids. **75**, 105 (2014)
47. S. Basu, S.K.M. Hossain, D. Chakravorty, M. Pal, Curr. Appl. Phys. **11**, 976 (2011)
48. K. Singh, S.K. Singh, D. Kaur, Ceram. Int. **42**, 13432 (2016)
49. T. Park, G.C. Papaefthymiou, A.J. Viescas, A.R. Moodenbaugh, S.S. Wong, Nano Lett. **7**, 766 (2007)
50. G. Tan, W. Yang, W. Ye, Z. Yue, H. Ren, A. Xia, J. Mater. Sci. **52**, 2694 (2017)